ADVANCED ENERGY MATERIALS
www.advenergymat.de

Enhanced Efficiency and Stability of Perovskite Solar Cells Through Nd-Doping of Mesostructured TiO_2

*Bart Roose, Karl C. Gödel, Sandeep Pathak, Aditya Sadhanala, Juan Pablo Correa Baena, Bodo D. Wilts, Henry J. Snaith, Ulrich Wiesner, Michael Grätzel, Ullrich Steiner, and Antonio Abate**

Block-copolymer templated chemical solution deposition is used to prepare mesoporous Nd-doped TiO_2 electrodes for perovskite-based solar cells. X-ray diffraction and photothermal deflection spectroscopy show substitutional incorporation into the TiO_2 crystal lattice for low Nd concentration, and increasing interstitial doping for higher concentrations. Substitutional Nd-doping leads to an increase in stability and performance of perovskite solar cells by eliminating defects and thus increasing electron transport and reducing charge recombination in the mesoporous TiO_2. The optimized doping concentration of 0.3% Nd enables the preparation of perovskite solar cells with stabilized power conversion efficiency of >18%.

1. Introduction

Solar energy is one of the leading candidates to meet the ever increasing demand for energy. The costs for solar energy production are however currently higher than other conventional and renewable energy sources.[1] Potentially lower cost alternatives to the currently used Si and GaAs based solar technologies[2] include solar cells that make use of mesoporous TiO_2 electrodes to collect and transport the electronic charges generated in metal–organic dyes, first demonstrated by O'Regan and Grätzel.[3] Since this first pioneering work, the performance of dye-sensitized TiO_2 solar cells (DSSCs) improved mainly by the development of new pigments that more effectively absorb the solar light spectrum.[4,5] A recent breakthrough was the introduction of organic–inorganic perovskites, which combine high light absorption with good charge transport.[6–12] The high perovskite conductivity enabled the exploration of new device architectures spanning from a perovskite-sensitized mesoporous TiO_2 to TiO_2-free planar heterojunction solar cells.[13] Currently, the best performing perovskite-based solar cells (PSCs), with a certified power conversion efficiency of more than 20%, employ a thin mesoporous TiO_2 layer as electron selective contact in combination with a thick solid perovskite absorber over-layer.[2]

Due to the favorable position of its conduction band (CB), a large band gap, long electron lifetimes and low fabrication costs, TiO_2 is frequently used to prepare mesoporous electrodes in several optoelectronic applications.[14–17] Nevertheless, the relatively high density of electronic trap states below the CB are a significant drawback for the application of TiO_2 electrodes in solar cells.[18] Indeed, trap states may have a large influence on charge recombination and charge transport, which in turn influence the solar cell voltage and current.[19–21] One method to reduce the trap states in TiO_2 is doping. A wide range of doping elements have been investigated for mesoporous TiO_2 electrodes in DSSCs[17,22–27] and more recently in PSCs.[28–31] Some dopants reduce the charge recombination[24] or increase electron transport in DSSCs[25] by reducing trap states below the CB. In addition to changes in the density of trap states, doping may induce a complex interplay of other effects that impact the device performance; for example, it can affect dye absorption or change the nanoparticle size and distribution and thereby the morphology of the mesostructured film, leading to a changed TiO_2-absorber interface area in DSSCs.[22] Furthermore, modifying the CB position by TiO_2 doping can either through a downward shift increase electron injection from the dye into the TiO_2[26] or through an upward shift increase the open-circuit voltage (V_{oc}).[27] These two effects however adversely affect each other. In PSCs, reduced recombination[28] and increased

B. Roose, Dr. B. D. Wilts, Prof. U. Steiner, Dr. A. Abate
Adolphe Merkle Institute
Chemin des Verdiers 4, CH-1700 Fribourg, Switzerland
E-mail: Antonio.abate@epfl.ch;
antonioabate83@gmail.com
K. C. Gödel, Dr. A. Sadhanala
Cavendish Laboratory
Department of Physics
University of Cambridge
J. J. Thomson Avenue, Cambridge CB3 0HE, UK
Dr. S. Pathak, Prof. H. J. Snaith
Clarendon Laboratory
Department of Physics
University of Oxford
Parks Road, Oxford OX1 3PU, UK
Dr. J. P. Correa Baena, Prof. M Grätzel, Dr. A. Abate
Swiss Federal Institute of Technology (EPFL)
Laboratory of Photonics and Interfaces
Station 6, CH-1015 Lausanne, Switzerland
Prof. U. Wiesner
Materials Science and Engineering
Cornell University
Ithaca, NY 14853, USA

DOI: 10.1002/aenm.201501868

electron transport[29] have been observed, as well as increased electron injection[29,30] or V_{oc}[28] through modification of the CB energy level. Another observed effect is the stabilization of the power output of PSCs, reducing the hysteresis of the device current-voltage characteristic.[31] Because dopants influence so many different properties of TiO_2 electrodes it is in general difficult to disentangle electronic (transport, recombination, CB shift) and morphological (particle size) contributions to the device performance.[17]

In a previous study we showed that aluminum (Al) doping increases stability in DSSCs by passivating oxygen defects in the TiO_2 lattice.[32] We demonstrated that oxygen defects not only limit electron transport within the TiO_2, but are also the cause of fast deterioration of solar cell performance upon UV irradiation. Therefore, DSSCs prepared with Al-doped TiO_2 were significantly more stable to UV exposure. However, the short-circuit current was significantly reduced as a result of a reduced charge injection from the dye into the TiO_2. This was attributed to the upward shift of the conduction band of TiO_2 by the newly introduced Al electron states.

In this study the stability and the performance of PSCs was improved by neodymium (Nd) doping of mesoporous TiO_2 films, which were employed as electron selective contact in PSCs. The Nd electron states are expected to have a negligible effect on the conduction band of TiO_2,[33] thus preventing the loss of photocurrent that was observed for Al doping. To study the electronic properties of the material independent of the film morphology, we use a block-copolymer templated solution based method which allows the preparation of identical mesoporous films irrespective of the Nd doping concentration. This way, we are able to demonstrate that Nd doping reduces the density of deep traps in the TiO_2 lattice, leading to reduced electron recombination, increased electron transport, and increased stability in PSCs. Nd-doped TiO_2 PSCs with a stabilized power output of more than 18% were manufactured.

2. Results

2.1. Characterization of Mesoporous TiO_2

2.1.1. Scanning Electron Microscopy (SEM)

A frequently observed phenomenon in doping studies is a decrease of the average TiO_2 particle size for doped samples,[34] leading to an increased TiO_2-absorber interface area, which results in improved DSSC performance. This however complicates the study of electronic properties of the materials as a function of dopant concentration. To exclude these morphological factors, we used the self-assembly of the amphiphilic block-copolymer polyisoprene-*block*-polyethyleneoxide (PI-*b*-PEO) to control the pore morphology during TiO_2 synthesis. The TiO_2 precursor complexes with the PEO block, yielding a porous network that is determined by the self-assembly of the polymer upon sample drying, calcination, and removal of the polymer.[35] The pore morphology is dictated by the molecular weight of the block-copolymer and the polymer-precursor concentration ratio, while the confinement of TiO_2 within the self-assembled morphology dictates the crystal size within polycrystalline TiO_2 network. The morphology obtained by block-copolymer templated assembly of TiO_2 is shown in **Figure 1**. An inverse micelle interconnected network with high porosity and surface area is formed during TiO_2 synthesis, where the pores are defined by the coil-size of the polyisoprene. Images and corresponding pore size distribution (D_p) of samples for all investigated doping concentrations show very similar morphologies with pore sizes of approximately 33 nm (Figure S1, Supporting Information, and **Table 1**).

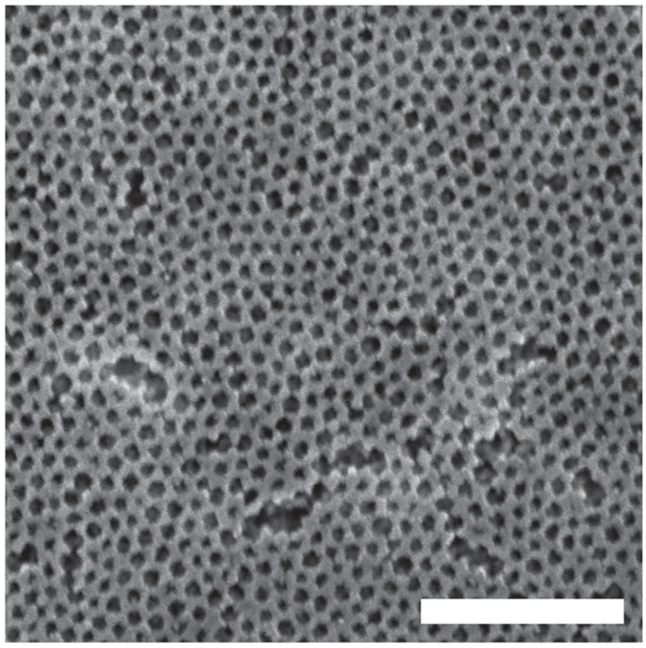

Figure 1. SEM image of a mesoporous TiO_2 electrode synthesized by a solution deposition process in which pore formation was controlled by the self-assembly of a block-copolymer. The film morphology and polycrystallinity is identical regardless of the Nd-doping level (see Figure S1, Supporting Information). Scale bar is 500 nm.

2.1.2. Crystal Structure

X-ray diffraction (XRD) was used to confirm the formation of anatase TiO_2. **Figure 2** shows the spectra for pristine, 0.3% and 0.5% Nd-doped TiO_2. All peaks can be assigned to anatase TiO_2 and no Nd_2O_3 peaks were observed, indicating that the Nd ions are incorporated in the TiO_2 lattice without disruption of the crystal structure.

Table 1. Pore size (D_p), crystallite size (D_p), and lattice parameters (*a* and *c*) for Nd-doped TiO_2. Pore size was extracted from the SEM images in Figure S1, Supporting Information. Crystallite size and lattice parameters were calculated using the equations in Figure S2, Supporting Information. The (100) peak of Si was used to calibrate the obtained spectra.

Nd [%]	D_p [nm]	D_c [nm]	*a* [Å]	*c* [Å]
0	33 ± 6	25.9 ± 0.5	3.763 ± 0.001	9.431 ± 0.002
0.3	33 ± 6	26.2 ± 0.9	3.766 ± 0.001	9.439 ± 0.002
0.5	34 ± 6	23.5 ± 0.8	3.766 ± 0.001	9.437 ± 0.002

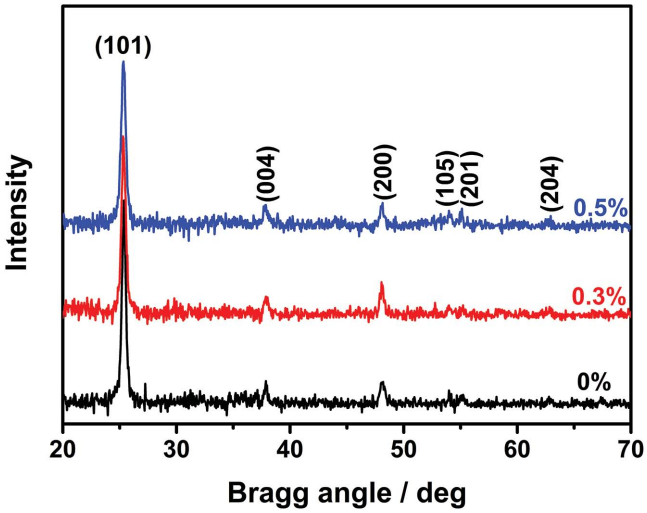

Figure 2. X-ray diffraction spectra of mesoporous films of undoped, 0.3% and 0.5% Nd-doped TiO_2. All peaks can be assigned to anatase TiO_2, indicating that Nd is incorporated into the TiO_2 lattice.

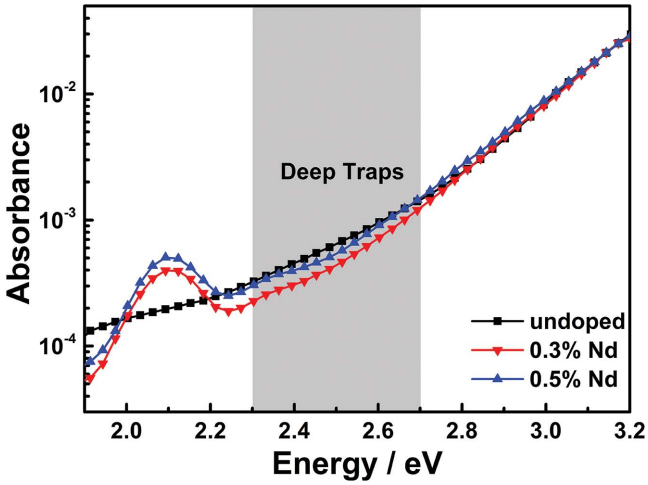

Figure 3. PDS spectrum of undoped, 0.3% and 0.5% Nd-doped TiO_2. Deep trap state energies are marked in gray. PDS is an ultrasensitive absorption technique that allows detecting absorbance values as low as 10^{-5}.

Because of the large difference in ionic radius between Nd^{3+} and Ti^{4+} (983 and 605 pm, respectively[36], the TiO_2 lattice expands upon substitutional incorporation of Nd^{3+}, resulting in a peak-shift to smaller angles. Interstitial doping has a much smaller effect on the lattice spacing.[37] Due to the large size of the Nd ion it is likely to be incorporated near the surface of TiO_2 crystallites. Lattice parameters and particle sizes were calculated according to equations reported in Section S2 of the Supporting Information. The values for the average size of crystallites (D_c) of the polycrystalline assembly and lattice parameters a and c are given in Table 1. D_p and D_c are similar (≈33 nm and ≈25 nm, respectively) for all doping concentrations, thus confirming that the block-copolymer templating not only preserves the morphology for the different doping levels, but also confines the crystallisation, preserving the crystal size. The lattice parameters for the doped samples show a unilateral increase from 3.763 to 3.766 Å for a and from 9.431 to 9.439 Å for c. The initial increase in lattice parameters suggests substitutional incorporation is dominant for 0.3% Nd-doped TiO_2. For 0.5% Nd, the lattice expansion is very similar to 0.3% doping, suggesting additional Nd is incorporated interstitially.

2.1.3. Electronic Properties

Photothermal deflection spectroscopy (PDS)[38] was used to probe sub-band gap states in undoped and doped TiO_2 as reported elsewhere.[39] **Figure 3** shows the PDS spectrum for TiO_2 with increasing Nd-doping concentration. The intraband gap state at 2.1 eV is attributed to the 4f transitions of Nd.[40] The peak intensity correlates with the doping concentration, indicating Nd is indeed increasingly incorporated into the TiO_2 lattice. Lanthanide induced intraband gap states are often associated with the up-conversion of low energy photons, making it possible to absorb photons that are otherwise lost.[41] Because of the low density of the intraband gap states and the low quantum efficiency of up-conversion processes it seems unlikely, however, that up-conversion contributes significantly to light absorption.

The band gap of TiO_2 is ≈3.2 eV, the energy levels of surface traps typically lie 0.5–0.7 eV below the conduction band (gray shading in Figure 3).[42,43] In Figure 3, the trap state density in this energy range is lowest for 0.3% Nd-doped TiO_2. A close-up of the deep trap state density for 0, 0.1%, 0.2%, 0.3%, 0.4%, and 0.5% can be found in Figure S3 of the Supporting Information. A minimum in deep trap state density is found for 0.3%. Because deep traps can act as recombination centers it is expected that the recombination rate for 0.3% Nd-doped TiO_2 is lower than that of pristine TiO_2.[18] For 0.5% Nd-doped TiO_2 the trap state density increases again, presumably because interstitial Nd ions acts as trap states, which is expected to lead to an increase in recombination and a loss in device performance.

2.2. Photovoltaic Performance

An initial doping concentration optimization in the range of 0%–0.5% Nd showed an increase in device performance up to 0.3% doping, after which the performance decreased. The results of this optimization can be found in Section S4 of the Supporting Information. Undoped, 0.3% and 0.5% devices were further optimized and studied in more detail to find the reason for the increase and subsequent decrease in device performance. The SEM image in **Figure 4**A shows the cross section of a photovoltaic device employing a ≈150 nm thick mesoporous layer of mesoporous TiO_2. The photocurrent–voltage (J–V) curves of the PSCs measured under AM1.5 simulated solar light (100 mW cm^{-2}) illumination are shown in Figure 4B. The photovoltaic parameters extracted from the J–V curves, the open-circuit potential (V_{oc}), short-circuit current (J_{sc}), fill factor (FF), power conversion efficiency (PCE), and the stabilized power output efficiency after 30 and 200 s are shown in **Table 2**. The maximum PCE is achieved for 0.3% Nd doped TiO_2, mainly through the improvement of the fill

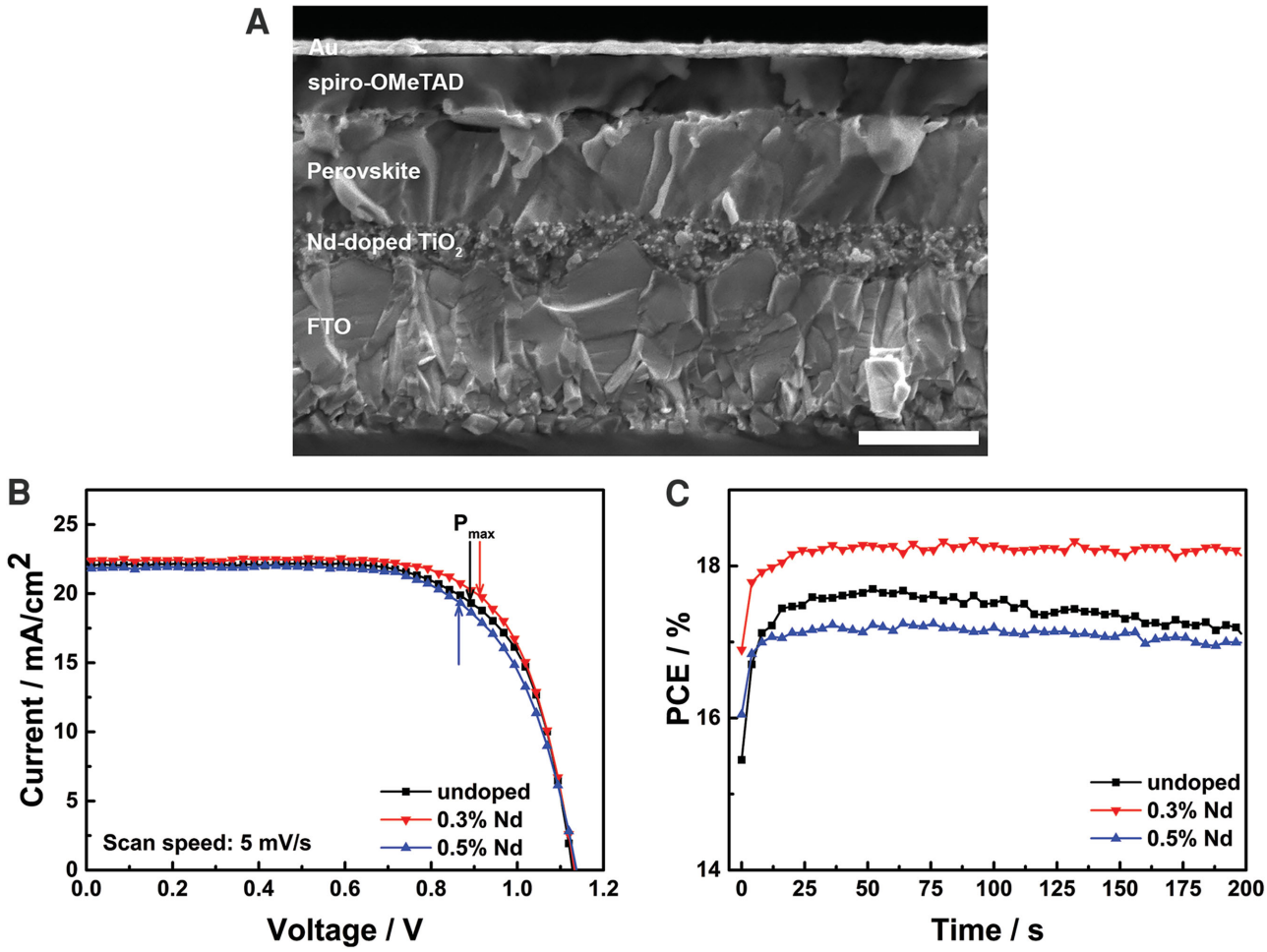

Figure 4. A) SEM cross-section of a photovoltaic device, scale bar is 500 nm; FTO transparent conductive electrode, compact TiO_2 electron blocking layer, 150–200 nm (Nd-doped) mesoporous TiO_2, perovskite capping layer, spiro-OMeTAD hole conducting layer and gold back contact. B) *J–V* curves for PSCs employing TiO_2, 0.3% Nd-doped TiO_2, and 0.5% Nd-doped TiO_2. The *J–V* curves were measured from forward bias to short circuit condition at the scan rate of 5 mV s^{-1} under AM1.5 simulated solar light (100 mW cm^{-2}) illumination. The cells were masked (0.16 cm^2) and characterized 2 d after their preparation. Table 2 lists the photovoltaic parameters for the three curves. C) Stabilized PCE of undoped, 0.3% Nd-doped and 0.5% Nd-doped TiO_2 PSCs. The voltage at the maximum power output was extracted from the *J–V* curves, the device was held at this voltage for 200 s to obtain the stabilized power output efficiency.

factor. In contrast to the earlier study employing Al doping in DSSCs,[32] no loss in J_{sc} was observed. This can be correlated to the fact that the Nd doping does not affect the TiO_2 band gap (Figure S6, Supporting Information) and the CB position, which would lead to a decrease in electron injection and a loss of J_{sc}.

The obtained efficiency in PSCs is dependent on the way the device is measured (preconditioning bias (light and voltage), voltage scan speed, and direction), so additional measurements are needed to verify the obtained PCE for device operation under realistic conditions. By determining the maximum power point and keeping the system at the corresponding voltage for

Table 2. Photovoltaic parameters of Nd-doped TiO_2: open-circuit voltage (V_{oc}), short-circuit current (J_{sc}), fill factor (FF), power conversion efficiency (PCE) extracted from the *J–V* curves in Figure 4B and stabilized power conversion efficiency (Stab. PCE) after 30 and 200 s, extracted from Figure 4C. Full statistics can be found in Figure S5, Supporting Information. The *J–V* characteristics were recorded at reverse bias at a scan rate of 5 mV s^{-1} across a 0.16 cm^2 aperture active area. The voltage at the maximum power output was extracted from the *J–V* curves and devices were then held at this voltage to determine the variation of the power output efficiency with time.

Nd [%]	V_{oc} [mV]	J_{sc} [mA cm^{-2}]	FF [%]	PCE [%]	Stab. PCE (after 30 s) [%]	Stab. PCE (after 200 s) [%]
0	1129	22.0	69.7	17.3	17.6	17.1
0.3	1133	22.3	71.6	18.1	18.2	18.2
0.5	1137	21.9	67.5	16.8	17.1	17.0

extended periods of time, a realistic PCE value can be determined.[44] Figure 4C shows the PCE at the maximum power point for the first 200 seconds, which demonstrates that steady-state conditions are achieved after approximately 30 s. We note that, regardless the doping level of TiO_2, the steady-state PCE is nearly identical to the PCE extracted from the J–V curves measured at 5 mV s^{-1}. These data confirm that the highest PCE is achieved for 0.3% Nd-doped TiO_2. A striking difference between the undoped and doped devices is the rapid decay of the device power output. For the undoped devices, the PCE initially increases and reaches a maximum after device operation for ≈50 s, followed by a rapid decrease in PCE. The 0.3% and 0.5% doped PSCs, on the other hand, remained stable for 200 s after the initial PCE increase. A 3 h stability test is shown in Figure S7 of the Supporting Information, here the initial rapid drop in PCE for undoped devices is again clearly shown, where it is absent for the doped devices. Such rapid losses in performance can be attributed to the UV-induced desorption of O_2 from oxygen vacancies in TiO_2.[45] Trivalent dopants, such as Al and Nd, have been shown to reduce the density of oxygen defects, thus inhibiting the PCE decay upon UV irradiation.[32]

In order to study the electronic properties of TiO_2 electrodes upon doping with Nd, we used intensity modulated photocurrent spectroscopy (IMPS)[46] and intensity modulated photovoltage spectroscopy (IMVS).[47] In PSCs the frequency overlap for charge transport in TiO_2 and perovskite may complicate the data interpretation. In order to circumvent this problem we prepared a set of solid state DSSCs sensitizing the Nd-doped and undoped mesoporous TiO_2 films with Y123-dye[48] and using spiro-OMeTAD as the hole transporting material, according to a method we reported previously.[49] Electron transport lifetimes for undoped, 0.3% Nd-doped and 0.5% Nd-doped samples are plotted against the short-circuit current in **Figure 5**A. A single exponential fit shows the transport lifetime evolution with the short-circuit current (J_{sc}). Electron transport is faster in the doped samples compared to the undoped analogues. This is in agreement with the increased performance of 0.3% Nd-doped devices. Faster charge transport leads to a lower series resistance, which in turn gives rise to the increase in the fill factor of Table 2. The effect is larger for low light intensities, again indicating a larger difference between the Nd-doped and undoped TiO_2 in deep trap state density, as deep trap states are filled at higher light intensities and contribute less to charge transport.[50] In Figure 5B, electron lifetimes are plotted against the open-circuit voltage (V_{oc}) for undoped, 0.3% and 0.5% Nd-doped TiO_2 samples. Electron lifetime is increased for the doped samples, indicating that charge recombination is reduced through the elimination of deep traps, resulting in an increase of V_{oc}. For 0.5% Nd-doped samples the electron lifetime is shorter than that of 0.3% Nd-doped samples. This indicates that the interstitially incorporated Nd sites can act as recombination centres, leading to a decreased device performance.

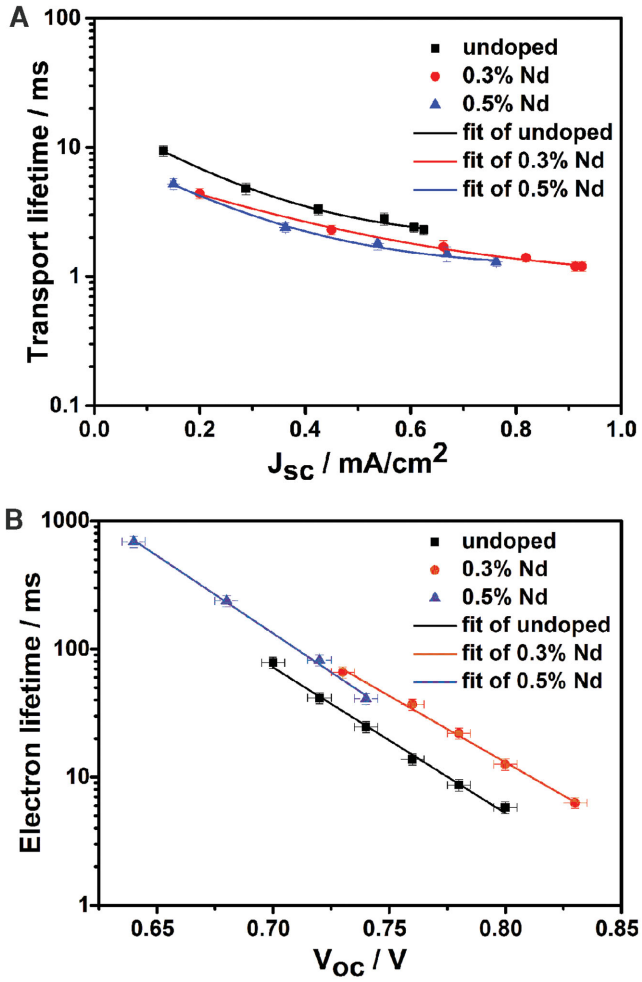

Figure 5. A) Electron transport lifetimes for undoped, 0.3% Nd-doped TiO_2 and 0.5% Nd-doped TiO_2 in solid state DSSCs as a function of the short-circuit current (J_{sc}), obtained through intensity modulated photocurrent spectroscopy (IMPS).[46] B) Electron lifetimes for undoped, 0.3% Nd-doped TiO_2 and 0.5% Nd-doped TiO_2 in solid state DSSCs as a function of open-circuit voltage (V_{oc}), obtained through intensity modulated photovoltage spectroscopy (IMVS).[47] The data are well fit by a single exponential (fit parameters are listed in Section S8 and S9, Supporting Information).

3. Conclusions

Polymer assisted sol–gel chemistry was used to prepare mesoporous Nd-doped TiO_2 electrodes. SEM, XRD, and PDS were employed to compare the resulting doped and undoped materials. Both interstitial and substitutional incorporation of Nd within the TiO_2 crystal lattice were observed. For 0.3% Nd content, substitutional doping was dominant. Upon increasing the doping concentration, the additional Nd ions were incorporated into interstitial sites. This was directly reflected in the PSC performance, which reached a maximum in power conversion efficiency for 0.3% Nd-doped mesoporous TiO_2 electrodes, mainly caused by an increase in the fill-factor, and deteriorated with higher doping levels. PDS, IMPS, and IMVS analysis elucidated this result by demonstrating the largest decrease in deep trap states, improved electron transport and reduced charge recombination for 0.3% Nd-doping. For 0.5% Nd-doping the deep trap state density increases again, leading to increased charge recombination and a drop in device performance. Furthermore, device power conversion efficiency was

maintained under continuous illumination. PSCs prepared with Nd-doped TiO_2 electrodes have higher early-time stability compared to undoped PSCs. Indeed, the optimized doping concentration of 0.3% Nd enabled 18% stabilized power conversion efficiency for 200 s in air, while undoped devices started to show a drop in performance after reaching a maximum around 50 s. The better lifetime of the doped devices is attributed to Nd passivation of oxygen defects, which in sealed devices play an important role in PSC degradation. In difference to earlier studies of Al-doping of TiO_2, Nd-doping increased the stability of PSCs without adversely affecting the short-circuit current of the devices.

4. Experimental Section

Material Characterization: Scanning electron microscopy was carried out on a Tescan MIRA 3 LMH with a field emission source operated at an acceleration voltage of 10 kV. X-ray diffraction was measured using a Bruker D8 θ/θ (fixed sample) spectrometer with a LynxEye position sensitive detector and a standard SC detector with autoabsorber and graphite 2nd beam monochromator. The spectrometer uses a Bragg Brentano parafocusing geometry and operates in reflection mode. Samples were deposited on Si-wafers and the (100) Si peak was used to calibrate the obtained spectra. PDS was measured with a Light Support MKII 100 W Xenon arc source coupled with a CVI DK240 monochromator. The probe beam comes from a Qioptiq 670 nm fiber-coupled diode laser.[51]

Solar Cell Preparation: Nippon Sheet Glass with FTO coating (10 Ω/sq) was cleaned by sonication in 2% Hellmanex solution for 30 min. After rinsing with deionized water and ethanol the substrates were treated with UV-ozone for 15 min. A 30 nm TiO_2 compact layer was deposited via spray pyrolysis at 450 °C from a precursor solution of titanium diisopropoxide bis(acetylacetonate) in anhydrous ethanol. After the spraying, the substrates were kept at 450 °C for 45 min before cooling down to room temperature. Mesostructured TiO_2 electrodes were synthesized using a structure directing block-copolymer.[35] A titanium precursor sol was prepared by adding 50 µL of HCl (37%) to 150 µL of titanium(IV) isopropoxide (TTIP) (Sigma-Aldrich, 99.999%) and stirred for 10 min. For the doped samples, neodymium(III) isopropoxide (Sigma-Aldrich, 99:8%) was dissolved in TTIP before the addition of HCl. The doping concentrations are given in terms of the Nd:Ti ratio. Subsequently, polyisoprene-block-polyethyleneoxide (PI-b-PEO) (50 mg, molar mass M_n = 34.4 kg mol^{-1}, 28 wt% PEO) was dissolved in 1 mL of azeotrope (72.84 wt% toluene and 27.16 wt% 1-butanol) and added to the precursor sol. After 20 h, the resulting solution was spin-coated (4000 rpm, 20 s) onto the FTO substrate. The films were annealed on a programmable hotplate (2000 W, Harry Gestigkeit GmbH) using a linear 2 h ramp to 600 °C followed by a dwell time of 1 h to remove the block-copolymer template and crystallize TiO_2. Perovskite and HTM were deposited according to literature.[52,53] Perovskite films were deposited from a precursor solution containing FAI (1 M), PbI_2 (1.1 M), MABr (0.2 M), and $PbBr_2$ (0.2 M) in anhydrous DMF:DMSO 4:1 (v:v). The perovskite solution was spin-coated in a two-step program at 1000 and 4000 rpm for 10 and 30 s, respectively. During the second step, 100 µL of chlorobenzene was poured onto the spinning substrate 15 s prior the end of the program. The substrates were then annealed at 100 °C for 1 h in a nitrogen glove box. Subsequently, the substrates were cooled down for a few minutes and a spiro-OMeTAD (Merck) solution (70×10^{-3} M in chlorobenzene) doped with bis(tri uoromethylsulfonyl)imide lithium salt (Li-TFSI, Aldrich), tris(2-(1H-pyrazol-1-yl)-4-tert-butylpyridine)-cobalt(III)tris(bis (tri uoromethylsulfonyl)imide) (FK209, Dyenamo), and 4-tert-butylpyridine (TBP, Aldrich) was spun at 4000 rpm for 20 s. The molar ratio of additives for spiro-OMeTAD was 0.5, 0.03, and 3.3 for Li-TFSI, FK209, and TBP, respectively. Finally, 70 nm of gold was thermally evaporated under high vacuum on top of the device.

Optoelectronic Measurements: For photovoltaic measurements, a solar simulator from ABET Technologies (Model 11016 Sun 2000) with a xenon arc lamp was used and the solar cell response was recorded using a Metrohm PGSTAT302N Autolab. The intensity of the solar simulator was calibrated to 100 mW cm^{-2} using a silicon reference cell from ReRa Solutions (KG5 filtered). *J–V* curves were measured in reverse bias (from high to low voltages), at a scan rate of 5 mV s^{-1}. The cells were masked to define the active area (0.16 cm^2) and were measured 2 d after their preparation. The voltage at the maximum power output was extracted from the *J–V* curves, the device was then held at this voltage to obtain the variation of the stabilized power output efficiency with time. IMPS was performed according to the procedure described in literature, using a 625 nm LED driver at different light intensities and a Metrohm PGSTAT302N Autolab.[47]

Supporting Information

Supporting Information is available from the Wiley Online Library or from the author.

Acknowledgements

A.A. received funding from the European Union's Seventh Framework Programme for research, technological development, and demonstration under Grant Agreement No. 291771. A.S. acknowledges funding and support from the Indo-UK APEX project. The authors acknowledge the Swiss National Science Foundation under Program NRP70 No. 153990.

Received: September 17, 2015
Revised: October 21, 2015
Published online: December 3, 2015

[1] T. M. Schmidt, T. T. Larsen-Olsen, J. E. Carlé, D. Angmo, F. C. Krebs, *Adv. Energy Mater.* **2015**, *5*, 1500569.
[2] NREL, Solar Cell Efficiency Chart, http://www.nrel.gov/ncpv/images/efficiency_chart.jpg (accessed: October 2015).
[3] B. O'Regan, M. Grätzel, *Nature* **1991**, *353*, 737.
[4] T. Kinoshita, J. T. Dy, S. Uchida, T. Kubo, H. Segawa, *Nat. Photonics* **2013**, *7*, 535.
[5] M.-W. Lee, J.-Y. Kim, H. J. Son, J. Y. Kim, B. Kim, H. Kim, D.-K. Lee, K. Kim, D.-H. Lee, M. J. Ko, *Sci. Rep.* **2015**, *5*, 7711.
[6] A. Kojima, K. Teshima, Y. Shirai, T. Miyasaka, *J. Am. Chem. Soc.* **2009**, *131*, 6050.
[7] H.-S. Kim, C.-R. Lee, J.-H. Im, K.-B. Lee, T. Moehl, A. Marchioro, S.-J. Moon, R. Humphry-Baker, J.-H. Yum, J. E. Moser, M. Grätzel, N.-G. Park, *Sci. Rep.* **2012**, *2*, 591.
[8] M. M. Lee, J. Teuscher, T. Miyasaka, T. N. Murakami, H. J. Snaith, *Science* **2012**, *338*, 643.
[9] J. Burschka, N. Pellet, S.-J. Moon, R. Humphry-Baker, P. Gao, M. K. Nazeeruddin, M. Grätzel, *Nature* **2013**, *499*, 316.
[10] M. Liu, M. B. Johnston, H. J. Snaith, *Nature* **2013**, *501*, 395.
[11] N. J. Jeon, J. H. Noh, W. S. Yang, Y. C. Kim, S. Ryu, J. Seo, S. I. Seok, *Nature* **2015**, *517*, 476.
[12] N. J. Jeon, J. H. Noh, Y. C. Kim, W. S. Yang, S. Ryu, S. I. Seok, *Nat. Mater.* **2014**, *13*, 897.
[13] O. Malinkiewicz, C. Roldan-Carmona, A. Soriano, E. Bandiello, L. Camacho, M. K. Nazeeruddin, H. J. Bolink, *Adv. Energy Mater.* **2014**, *4*, 1400345.
[14] D. Y. â. C. Leung, X. Fu, C. Wang, M. Ni, M. K. â. H. Leung, X. Wang, X. Fu, *ChemSusChem* **2010**, *3*, 681.
[15] M. A. Rauf, M. A. Meetani, S. Hisaindee, *Desalination* **2011**, *276*, 13.

[16] H. Park, Y. Park, W. Kim, W. Choi, *J. Photochem. Photobiol. C: Photochem. Rev.* **2013**, *15*, 1.
[17] B. Roose, S. Pathak, U. Steiner, *Chem. Soc. Rev.*, **2015**, *44*, 8326.
[18] H. J. Snaith, L. Schmidt-Mende, *Adv. Mater.* **2007**, *19*, 3187.
[19] H. K. Ardakani, *Thin Solid Films* **1994**, *248*, 234.
[20] A. T. Paxton, L. Thien-Nga, *Phys. Rev. B* **1998**, *57*, 1579.
[21] Y. Wang, D. Wu, L.-M. Fu, X.-C. Ai, D. Xu, J.-P. Zhang, *ChemPhysChem* **2015**, *16*, 2253.
[22] B. Choudhury, B. Borah, A. Choudhury, *Mater. Sci. Eng. B* **2013**, *178*, 239.
[23] A. K. Chandiran, F. Sauvage, F. M. Casas-Cabanas, P. Comte, S. M. Zakeeruddin, M. Grätzel, *J. Phys. Chem. C* **2010**, *114*, 15849.
[24] K. H. Ko, Y. C. Lee, Y. J. Jung, *J. Colloid Interface Sci.* **2005**, *283*, 482.
[25] J. Liu, Y. Duan, X. Zhou, Y. Lin, *Appl. Surf. Sci.* **2013**, *277*, 231.
[26] M. Wang, S. Bai, A. Chen, Y. Duan, Q. Liu, D. Li, Y. Lin, *Electrochim. Acta* **2012**, *77*, 54.
[27] C. Zhang, S. Chen, L. Mo, Y. Huang, H. Tian, L. Hu, Z. Huo, S. Dai, F. Kong, X. Pan, *J. Phys. Chem. C* **2011**, *115*, 16418.
[28] J. Wang, M. Qin, H. Tao, W. Ke, Z. Chen, J. Wan, P. Qin, L. Xiong, H. Lei, H. Yu, G. Fang, *Appl. Phys. Lett.* **2015**, *106*, 121104.
[29] D. H. Kim, G. S. Han, W. M. Seong, J.-W. Lee, B. J. Kim, N.-G. Park, K. S. Hong, S. Lee, H. S. Jung, *ChemSusChem* **2015**, *8*, 2392.
[30] H. Zhou, Q. Chen, G. Li, S. Luo, T. Song, H.-S. Duan, Z. Hong, J. You, Y. Liu, Y. Yang, *Science* **2014**, *345*, 542.
[31] H. Nagaoka, F. Ma, D. W. deQuilettes, S. M. Vorpahl, M. S. Glaz, A. E. Colbert, M. E. Ziffer, D. S. Ginger, *J. Phys. Chem. Lett.* **2015**, *6*, 669.
[32] S. K. Pathak, A. Abate, P. Ruckdeschel, B. Roose, K. C. Gödel, Y. Vaynzof, A. Santhala, S.-I. Watanabe, D. J. Hollman, N. Noel, A. Sepe, U. Wiesner, R. Friend, H. J. Snaith, U. Steiner, *Adv. Funct. Mater.* **2014**, *24*, 6046.
[33] Q. Yao, J. Liu, Q. Peng, X. Wang, Y. Li, *Chem. Asian J.* **2006**, *1*, 737.
[34] C. J. Brinker, G. W. Scherer, *Sol-Gel Science, the Physics and Chemistry of Sol-Gel Processing*, Academic Press, Boston, MA **1990**.
[35] S. Guldin, P. Docampo, M. Stefik, G. Kamita, U. Wiesner, H. J. Snaith, *Small* **2012**, *8*, 432.
[36] R. Shannon, *Acta Crystallogr., Sect. A* **1976**, *32*, 751.
[37] A. Burns, G. Hayes, W. Li, J. Hirvonen, J. D. Demaree, S. I. Shah, *Mater. Sci. Eng. B* **2004**, *111*, 150.
[38] S. E. Bialkowski, *Photothermal Spectroscopy Methods for Chemical Analysis*, John Wiley & Sons, Hoboken, NJ, USA **1996**.
[39] K. C. Gödel, Y. C. Choi, B. Roose, A. Sadhanala, H. J. Snaith, S. I. Seok, U. Steiner, S. K. Pathak, *Chem. Commun.* **2015**, *51*, 8640.
[40] N. Wang, W. Jiang, X. Xu, Z. Si, H. Bai, C. Tian, *Anal. Sci.* **2002**, *18*, 591.
[41] S. H. Huang, *J. Am. Ceram. Soc.* **2013**, *96*, 3108.
[42] G. Redmond, D. Fitzmaurice, M. Grätzel, *J. Phys. Chem.* **1993**, *97*, 6951.
[43] G. Boschloo, D. Fitzmaurice, *J. Phys. Chem. B* **1999**, *103*, 2228.
[44] H. J. Snaith, A. Abate, J. M. Ball, G. E. Eperon, T. Leijtens, N. K. Noel, S. D. Stranks, J. T.-W. Wang, K. Wojciechowski, W. Zhang, *J. Phys. Chem. Lett.* **2014**, *5*, 1511.
[45] T. Leijtens, G. E. Eperon, S. Pathak, A. Abate, M. M. Lee, H. J. Snaith, *Nat. Commun.* **2013**, *4*, 2885.
[46] F. Cao, G. Oskam, G. J. Meyer, P. C. Searson, *J. Phys. Chem.* **1996**, *100*, 17021.
[47] P. R. F. Barnes, K. Miettunen, X. Li, A. Y. Anderson, T. Bessho, M. Grätzel, B. C. O'Regan, *Adv. Mater.* **2013**, *25*, 1881.
[48] H. N. Tsao, C. Yi, T. Moehl, J. H. Yum, S. M. Zakeeruddin, M. K. Nazeeruddin, M. Grätzel, *ChemSusChem* **2011**, *4*, 591.
[49] A. Abate, S. Paek, F. Giordano, J. P. Correa Baena, M. Saliba, P. Gao, T. Matsui, J. Ko, S. M. Zakeeruddin, K. H. Dahmen, A. Hagfeldt, M. Grätzel, M. K. Nazeerudding, *Energy Environ. Sci.* **2015**, *8*, 2946.
[50] G.-O. Kim, K.-S. Ryu, *Bull. Korean Chem. Soc.* **2012**, *33*, 469.
[51] A. Sadhanala, F. Deschler, T. H. Thomas, S. E. Dutton, K. C. Goedel, F. C. Hanusch, M. L. Lai, U. Steiner, T. Bein, P. Docampo, D. Cahen, R. H. Friend, *J. Phys. Chem. Lett.* **2014**, *5*, 2501.
[52] A. Abate, T. Leijtens, S. Pathak, J. Teuscher, R. Avolio, M. E. Errico, J. Kirkpatrik, J. M. Ball, P. Docampo, I. McPherson, H. J. Snaith, *Phys. Chem. Chem. Phys.* **2013**, *15*, 2572.
[53] A. Abate, D. R. Staff, D. J. Hollman, H. J. Snaith, A. B. Walker, *Phys. Chem. Chem. Phys.* **2014**, *16*, 1132.